Electron Glass Phase with Resilient Zhang-Rice Singlets in $LiCu_3O_3$

A. Consiglio,[1] G. Gatti,[2,3] E. Martino,[2] L. Moreschini,[4,5,6] J. C. Johannsen,[2] K. Prša,[2,7] P. G. Freeman,[2,8] D. Sheptyakov,[7] H. M. Rønnow,[2] R. Scopelliti,[9] A. Magrez,[2] L. Forró,[2,10] C. Schmitt,[11] V. Jovic,[4,12] C. Jozwiak,[4] A. Bostwick,[4] E. Rotenberg,[4] T. Hofmann,[1] R. Thomale,[1] G. Sangiovanni,[1] D. Di Sante,[13] M. Greiter,[1] M. Grioni,[2] and S. Moser[2,4,11,*]

[1]*Institut für Theoretische Physik und Astrophysik and Würzburg-Dresden Cluster of Excellence ct.qmat, Universität Würzburg, 97074 Würzburg, Germany*
[2]*Institute of Physics, Ecole Polytechnique Fédérale de Lausanne (EPFL), CH-1015 Lausanne, Switzerland*
[3]*Department of Quantum Matter Physics, University of Geneva, 24 Quai Ernest-Ansermet, 1211 Geneva, Switzerland*
[4]*Advanced Light Source (ALS), Berkeley, California 94720, USA*
[5]*Materials Sciences Division, Lawrence Berkeley National Laboratory, Berkeley, California 94720, USA*
[6]*Department of Physics, University of California, Berkeley, Berkeley, California 94720, USA*
[7]*Laboratory for Neutron Scattering and Imaging, Paul Scherrer Institut, 5232 Villigen PSI, Switzerland*
[8]*Jeremiah Horrocks Institute for Mathematics, Physics and Astronomy, University of Central Lancashire, Preston PR1 2HE, United Kingdom*
[9]*Institute of Chemical Sciences and Engineering, Ecole Polytechnique Fédérale de Lausanne (EPFL), CH-1015 Lausanne, Switzerland*
[10]*Stavropoulos Center for Complex Quantum Matter, Department of Physics and Astronomy, University of Notre Dame, Notre Dame, Indiana 46556, USA*
[11]*Physikalisches Institut and Würzburg-Dresden Cluster of Excellence ct.qmat, Universität Würzburg, Würzburg 97074, Germany*
[12]*Earth Resources and Materials, Institute of Geological and Nuclear Science, Lower Hutt 5010, New Zealand and MacDiarmid Institute for Advanced Materials and Nanotechnology, Wellington 6012, New Zealand*
[13]*Department of Physics and Astronomy, University of Bologna, Bologna, Italy*

(Received 31 July 2023; accepted 12 February 2024; published 20 March 2024)

$LiCu_3O_3$ is an antiferromagnetic mixed valence cuprate where trilayers of edge-sharing Cu(II)O ($3d^9$) are sandwiched in between planes of Cu(I) ($3d^{10}$) ions, with Li stochastically substituting Cu(II). Angle-resolved photoemission spectroscopy (ARPES) and density functional theory reveal two insulating electronic subsystems that are segregated in spite of sharing common oxygen atoms: a Cu d_{z^2}/O p_z derived valence band (VB) dispersing on the Cu(I) plane, and a Cu $3d_{x^2-y^2}$/O $2p_{x,y}$ derived Zhang-Rice singlet (ZRS) band dispersing on the Cu(II)O planes. First-principle analysis shows the Li substitution to stabilize the insulating ground state, but only if antiferromagnetic correlations are present. Li further induces substitutional disorder and a 2D electron glass behavior in charge transport, reflected in a large 530 meV Coulomb gap and a linear suppression of VB spectral weight at E_F that is observed by ARPES. Surprisingly, the disorder leaves the Cu(II)-derived ZRS largely unaffected. This indicates a local segregation of Li and Cu atoms onto the two separate corner-sharing $Cu(II)O_2$ sub-lattices of the edge-sharing Cu(II)O planes, and highlights the ubiquitous resilience of the entangled two hole ZRS entity against impurity scattering.

DOI: 10.1103/PhysRevLett.132.126502

The principal oxides of copper, cuprous oxide, and cupric oxide, widely differ in their electronic properties [1]. Cu_2O contains Cu(I) with a completely filled Cu $3d$ shell and is a nonmagnetic band insulator. CuO, however, contains Cu(II) with an open Cu $3d^9$ shell and is an antiferromagnetic (AFM) charge-transfer insulator [2]. Its lowest energy hole excitations have mixed $3d^9\underline{L}$ and $3d^8$ character ($\underline{L}$: ligand oxygen hole) [3,4] that are still a matter of debate [5].

In the low dimensional cuprates, Cu(II) is typically coordinated by four oxygens, forming rectangular CuO plaquettes [Fig. 1(c)]. These constitute building blocks of one- (1D) or two-dimensional (2D) networks, with adjacent plaquettes sharing either one (corner sharing) or two oxygens (edge sharing). In the corner-sharing configuration, the angle of the Cu-O-Cu bond is close to 180°, inducing superexchange interaction and antiferromagnetism [6]. Doping a low-energy hole into the O $2p$ sublattice, its spin entangles with the Cu $3d_{x^2-y^2}$ hole, forming a local singlet of $^1A_1$ symmetry and mainly $d^9\underline{L}$ character, with each hole in b_{1g} symmetric one-particle wave functions (one in Cu $d_{x^2-y^2}$, the other in a linear combination of O $p_{x,y}$) [3,7]. This entangled two-hole quasiparticle (QP), dubbed Zhang-Rice singlet (ZRS), effectively disperses on the 2D Cu(II) sublattice assuming a bandwidth that is

proportional to the superexchange energy $J \sim 4t^2/U \sim$ 130 meV, described by effective one band Hubbard or t-J Hamiltonians [3,4,8]. While this establishes the spectral equivalence of the ZRS and a one-electron excitation, their eigenstate profiles still differ substantially. As a consequence, phenomena that involve the explicit spatial distribution of the ZRS QP, such as impurity scattering, are subject to significant corrections. In the edge sharing configuration, the Cu-O-Cu bond angle is close to 90° and the superexchange interaction is suppressed to values $J \sim 10$ meV [6,9–11]. ZRS wave functions of adjacent plaquettes are thus orthogonal, and a ZRS dispersion cannot stabilize [12,13].

Coupling a Cu(II)-oxide to Cu(I) adds additional complexity and can lead to novel electronic phenomena. This was recently exemplified by ARPES experiments on $LiCu_2O_2$, a mixed-valence compound where 1D edge-sharing chains of $Cu(II)O_4$ are coupled to 2D square lattices of Cu(I) through hybridization with common oxygens [14]. While the Cu(I) and Cu(II) based structural subunits retain their individual electronic character, the electronic structure was still found to be nontrivial, with an experimental bandwidth broadening of the Cu(I)-derived valence band (VB) of 250% with respect to predictions of density functional theory (DFT). The purely edge-sharing $Cu(II)O_2$ chains in $LiCu_2O_2$, however, do not support the ZRS. We thus anticipate intriguing electronic effects in materials combining corner-sharing 2D networks of Cu(II)O with Cu(I).

Such a system is embodied in $LiCu_3O_3$, the least studied member within the lithium copper oxide family. Its tetragonal crystal structure (P4/mmm, $a = 2.81$ Å, $c = 8.89$ Å) is shown in Fig. 1(a) [15–18]. Ignoring the lithium, the 3D unit cell (UC, black) consists of trilayers of Cu(II)O [Fig. 1(c)] sandwiched between square lattice planes of Cu(I) [Fig. 1(b)]. The trilayers are structurally similar to tetragonal copper oxide (T-CuO), an epitaxial stack of Cu(II)O planes with both edge- and corner-sharing properties [12], yet with smaller out-of-plane to in-plane Cu(II)-O bond-length ratio of 1.22 vs 1.37 in T-CuO. Because of the c-axis staggering [Fig. 1(a)], the Cu(II) of Cu2 and the Cu(I) of Cu1 share common oxygen ligands within the two equivalent Cu3 planes. As we show here, $LiCu_3O_3$ is thus a hybrid containing a renormalized Cu(I)-derived VB similar to $LiCu_2O_2$ [14] that is electronically separated from a Cu(II)O-derived ZRS as found in T-CuO [12].

The lithium stochastically substitutes the Cu(II) species and adds additional complexity, with ~20% Li per Cu site in Cu2, and ~40% Li per Cu site in the Cu3 plane [15,16,18]. As seen in Figs. 1(d) and 1(e), this disorder—along with long range Coulomb interactions—governs the temperature dependence of dc current. In particular, the in-plane resistivity ρ_{ab} scales according to an Efros-Shklovskii variable range hopping law $\rho \propto \exp(\sqrt{T_0/T})$ [19,53,54] with characteristic temperature

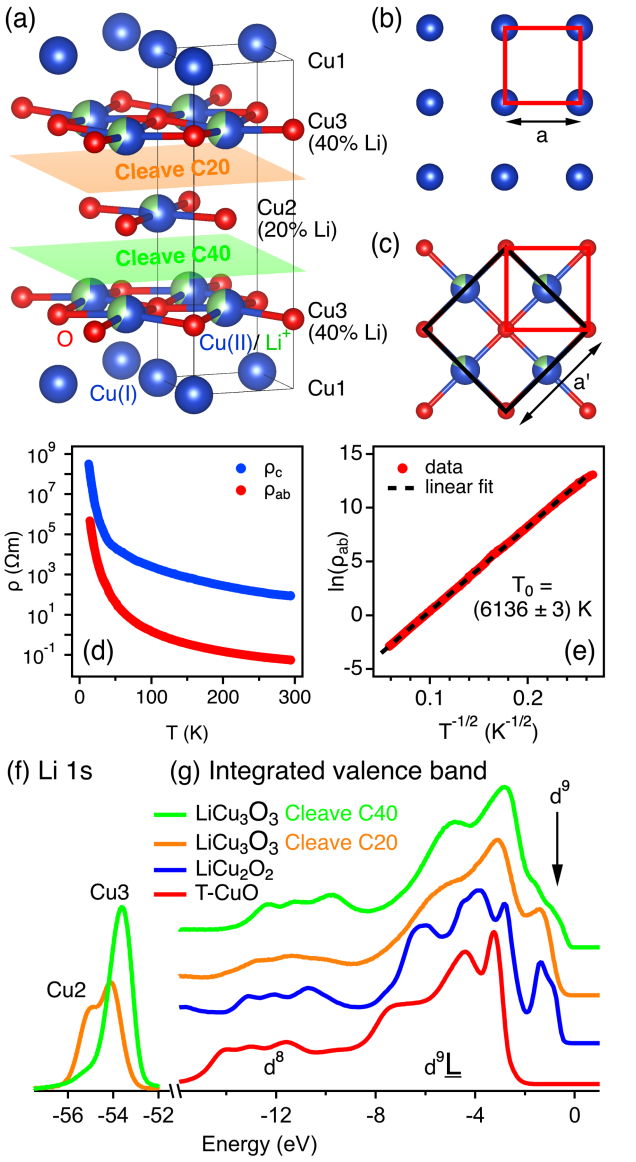

FIG. 1. (a) $LiCu_3O_3$ crystal structure, UC and natural cleavage planes. (b) Cu(I) form a square lattice with periodicity a (red square). (c) In a Cu(II) plane, edge-sharing CuO_4 plaquettes form a 2D square lattice with the same periodicity. The black square is the non-primitive $c(2 \times 2)$ UC. Li stochastically substitutes Cu(II) according to the stoichiometric ratios in (a). (d) In-plane (red) and out-of-plane (blue) DC resistivity of $LiCu_3O_3$. (e) The natural logarithm of the in plane resistivity scales as $T^{-1/2}$ with slope $\sqrt{T_0}$. (f) Li 1s spectra of both $LiCu_3O_3$ cleaves ($h\nu = 100$ eV). (g) Integrated VB spectra of both $LiCu_3O_3$ cleaves, compared to results from $LiCu_2O_2$ (blue [14]) and T-CuO (red [12]).

$T_0 = (6136 \pm 3)$ K, demonstrating the presence of a $k_B T_0 \sim$ 530 meV Coulomb gap from 15 to 300 K. T_0 also provides an upper bound of the charge carriers' localization length $\xi \leq 1.7$ nm $\sim 6a$ [18,20,21], which indicates strong charge localization and in-plane conduction to be dominated by slow hopping rather than fast diffusion processes [18]. Out-of-plane resistivity ρ_c exceeds ρ_{ab} by 2–3 orders of

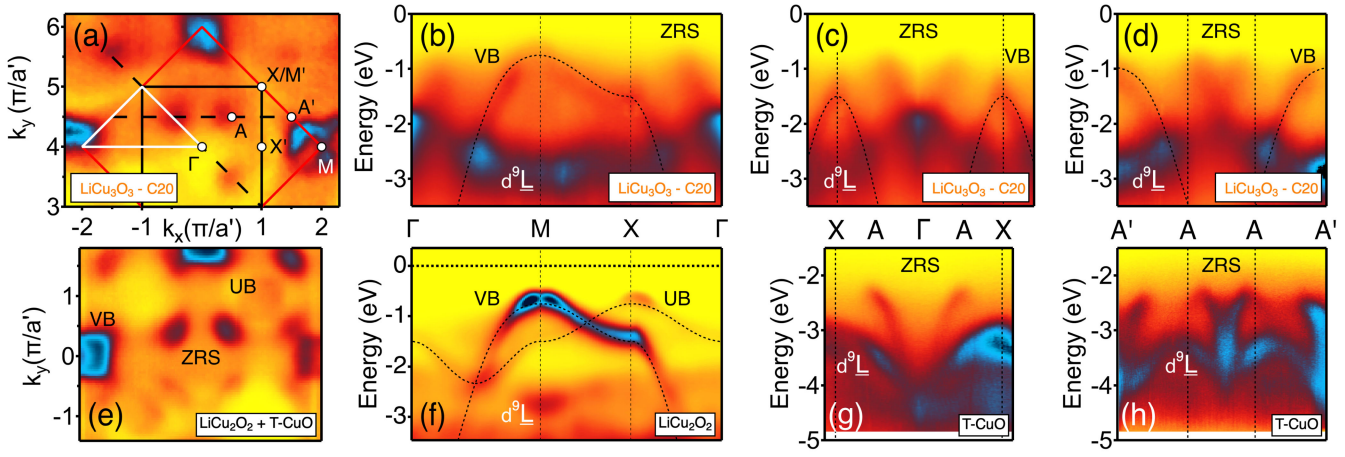

FIG. 2. (a) ARPES CE map of $LiCu_3O_3$—C20 ($h\nu = 150$ eV, $T = 150$ K) at $E = -0.7$ eV. Red and black squares are BZs corresponding to the UCs defined in Fig. 1(c). As at normal photo-electron emission, the ZRS is suppressed [12,60], we show data centered around $(k_x, k_y) = (0, 4\pi/a')$. (b) ARPES dispersion along the white triangular path in (a), compared to results from $LiCu_2O_2$ in (f). The latter also exhibits an umklapp band (UB) not present in $LiCu_3O_3$ [14]. (c) and (d) Dispersions along the black dashed lines in (a), and compare directly to the ZRS of T-CuO in (g) and (h) [12]. (e) Artificial sum of ARPES CE cuts of $LiCu_2O_2$ [14] and T-CuO [12].

magnitude, showing these hopping processes to take place predominantly in the plane [18,22,55]. $LiCu_3O_3$ thus lends itself as a 2D electron glass, i.e., an Anderson insulator subject to strong disorder and Coulomb interactions [20,21,23,56].

Despite the impact of substitutional disorder on transport, neutron scattering and SQUID magnetization measurements show Cu(II) derived long-range AFM order below $T_N \sim 124$ K [18]. ARPES reveals both the Cu(I) VB and the Cu(II)O ZRS bands to remain surprisingly intact—a phenomenon that exact diagonalization (ED) and DFT calculations ascribe to a kinetic energy driven segregation of Li and Cu(II) species onto separate corner-sharing CuO_2 sublattices. The VB, however, exhibits a soft, linear Coulomb gap when tuned to the Fermi energy (E_F), consistent with the electron glass scenario suggested by transport [24,57].

Let us focus on the Li 1s angle integrated photoemission spectra of $LiCu_3O_3$ single crystals cleaved in ultrahigh vacuum [Fig. 1(f)]. We distinguish two natural cleavage planes that terminate $LiCu_3O_3$ with planes Cu2 (cleave C20) and Cu3 (cleave C40), respectively [Fig. 1(a)]. While C20 reveals two peaks related to Li species in both the Cu2 (−55.08 eV) and the underlying Cu3 planes (−54.05 eV), C40 exhibits the single Li peak of Cu3 (−53.60 eV), shifted by ∼0.4 eV to lower binding energy with respect to C20, due to rigid surface band bending [58]. VB spectra of both terminations in Fig. 1(g) compare well to results obtained on T-CuO [12] and $LiCu_2O_2$ [14], exhibiting the characteristic of a correlated charge transfer insulator: a manifold of Cu(II)-derived d^8 states at ~ -12 eV and an O-derived $d^9\underline{L}$ band around ~ -4 eV. Consistent with the Li 1s core level, the VB features of C40 are shifted upwards with respect to C20, with finite spectral weight at E_F leading to charge screening that produces the asymmetry in the Li 1s peak [59]. Distinct from T-CuO, both $LiCu_2O_2$ and $LiCu_3O_3$ exhibit additional features within the charge-transfer gap (arrow).

We examine these features in the ARPES constant energy (CE) map of Fig. 2(a), taken from C20 at $E = -0.7$ eV. In addition to the primitive Brillouin zone (BZ, red square) and high symmetry points of $LiCu_3O_3$, and consistent with our notation for T-CuO in Ref. [12], we define the midpoint X' between Γ and M (the X point of the reduced BZ of a corner-sharing CuO_2 sublattice, black), and pairs of points A, A' that are symmetric with respect to the XX' X line. We observe two sets of spectral features: First, intense spectral contours centered at the M points of the primitive BZ reflect the periodicity of the crystallographic surface UC [red in Figs. 1(b) and 1(c)]. Second, weaker spectral lobes are observed at the A points, i.e., at $(\pm\pi/2a', \pm\pi/2a')$ with respect to the reduced BZ, corresponding to a $\sqrt{2}$ times larger and 45° rotated real space UC with lattice constant $a' = a\sqrt{2}$ [black in Fig. 1(c)]. The band dispersion along the ΓMXΓ path [white triangle in Fig. 2(a)] in Fig. 2(b) shows two sets of bands [18]: First, a VB of bandwidth ∼3.4 eV and maximum at ~ -0.7 eV that forms the contours at M in panel (a). By analogy with $LiCu_2O_2$ in Fig. 2(f) [14] and confirmed by DFT [18], this band is of mostly Cu(I) d_{z^2} and adjacent O p_z character, and emerges from a broad $d^9\underline{L}$ manifold at around −2.3 eV [4]. Second, faint lobes at A and A' in panel (a) mark the onset of the ZRS at ~ -0.7 eV in (b) [2]. As seen in the E vs $k_{\|}$ cuts of panels (c),(d), it is similar to the ZRS in T-CuO shown in (g),(h), where the Cu(II) atoms also form mixed edge and corner-sharing CuO planes. Both VB and ZRS exhibit negligible k_z dispersion in ARPES and are thus clearly 2D [18].

Based on these experimental observations, we conjecture the low-energy electronic structure of $LiCu_3O_3$ to host two

segregated electronic subsystems: (i) a ZRS band primarily associated to Cu(II) $d_{x^2-y^2}$ and O $p_{x,y}$ orbitals that propagates on the Cu(II)O planes and shows a similar dispersion as in T-CuO; and (ii) a VB of Cu(I) d_{z^2} and O p_z orbital character that propagates on the Cu(I) lattice and displays a similar bandwidth and dispersion as in $LiCu_2O_2$. Indeed, the resemblance of Fig. 2(a) with an artificial sum of $LiCu_2O_2$ [14] and T-CuO [12] data in Fig. 2(e) illustrates the composite nature of the $LiCu_3O_3$ electronic structure [61].

Surprises come at a close inspection of ARPES measured on C40. A CE map in Fig. 3(a), this time collected at −0.4 eV, is similar to the CE map of C20 at −0.7 eV in Fig. 2(a), showing both the onset of the Cu d_{z^2}/O p_z derived VB and of the Cu $3d_{x^2-y^2}$/O $2p_{x,y}$ derived ZRS. In contrast to C20, however, upwards surface band bending—as commonly present in transition metal insulators [58]—renders the VB slightly p doped, producing the remnant Fermi surface shown in panel (b). An ARPES cut along the dashed line in (b) shows spectral weight to not quite reach, and in fact, even repel from E_F, resulting in a *squashed* VB maximum in panel (c). An energy distribution curve (EDC, red line) of the VB at $k_x = 0$ in Fig. 3(e) appears linearly suppressed close to E_F (dashed line). While not strictly zero around $E_F \pm k_B T$ due to thermal smearing, such a linear suppression of intensity $\propto |E - E_F|$ is at odds with the Fermi liquid picture, where a Lorentzian QP line shape $\Gamma/[(E - E_F)^2 + \Gamma^2]$ with inverse QP lifetime Γ, multiplied by the Fermi function, is expected. It is, however, reminiscent of the soft Coulomb gap expected in an electron glass and thus consistent with the Efros-Shklovskii scaling observed in transport [19–21,25,53,62,63].

Depositing potassium (K) onto C40 induces a downwards band bending and repopulates the VB, consistent with the gradual retraction of the VB from E_F observed in the EDCs of Fig. 3(e). A line shape comparison of all normalized and shifted EDCs in Fig. 3(f) outlines how the initial linear onset (red) transitions to a Lorentzian line shape (blue) upon the VB populating and crossing the mobility edge. The filled VB is shown in panel (d) and traces a parabolic band maximum similar to what we observe for C20. Further, Fig. 3(g) shows a consecutive suppression of the Li 1s high energy tail [cf. Fig. 1(f)] with electron doping. This underlines the gradual depletion of the Fermi sea and a consequent reduction of core hole screening upon VB filling and the surface becoming insulating as described in Ref. [59].

Finally, we notice that despite the ∼40% Li disorder of cleave C40 as compared to ∼20% of C20, Figs. 2(a) and 3(a) show essentially equally pronounced ZRS lobes. This is consistent with ED and DFT calculations, which find the closed shell Li^+ ions to contribute no or only very little kinetic energy to the QP hopping via O $2p_{x,y}$ orbitals [18]. The system thus tends to maximize the number of unperturbed 180° Cu-O-Cu bonds each contributing one J in

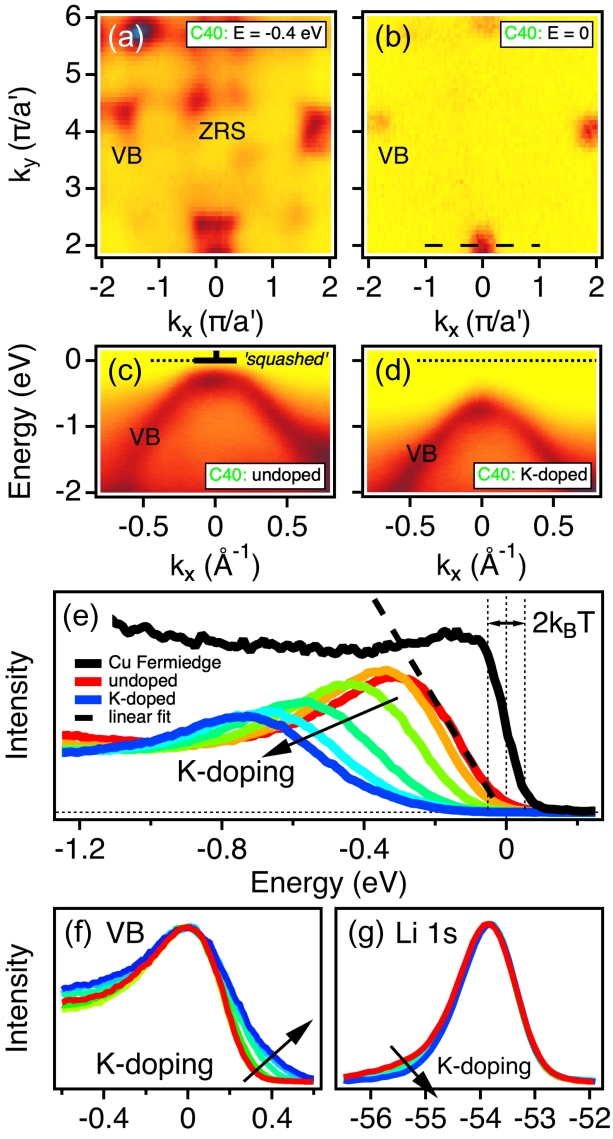

FIG. 3. ARPES CE maps of $LiCu_3O_3$—C40 ($h\nu = 150$ eV, $T = 300$ K) at (a) $E = -0.4$ eV and (b) $E = 0 = E_F$. (c) VB dispersion along the black dotted path in (b). (d) K deposition shifts the VB and recovers a parabolic dispersion. (e) EDC at $k_x = 0$ as a function of K deposition. The undoped EDC (red line) exhibits a linear suppression indicative of a Coulomb gap (cf. Fermi edge of poly-crystalline Cu, black). K doping shifts the VB towards higher energies and recovers a Lorentzian, as highlighted by the line shape comparison in (f). (g) The (bad) metal to insulator transition of the VB is accompanied by a suppression of the shoulder in Li 1s [59].

energy, and Li locally segregates onto one out of the two available CuO_2 sublattices [Fig. 4(a)], while the ZRS stabilizes on the other. Statistical nucleation of Li and Cu atoms during crystal growth then solely demands the recurring formation of domain walls across which Li changes sublattice. Out of four conceivable geometries designed according to these energy criteria, ED and DFT find the alternating 3 leg ladder in Fig. 4(b) to be

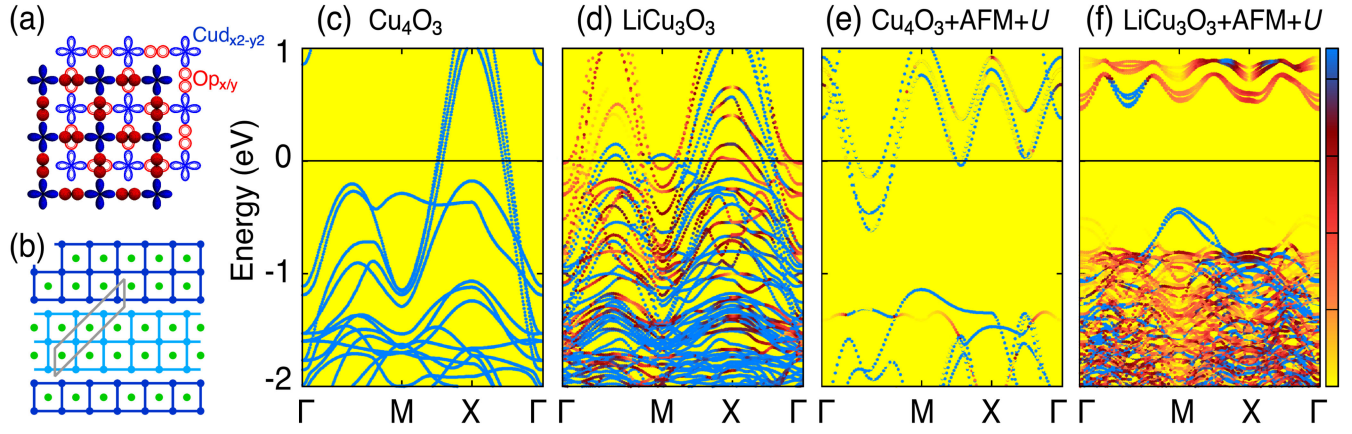

FIG. 4. (a) Decomposition of the CuO plane into two corner-sharing CuO_2 sublattices. The ZRS is formed from Cu $d_{x^2-y^2}$ (blue) and O $p_{x,y}$ (red) orbitals. (b) Energetically most favorable periodic ordering motif of a Cu3 plane (40% Li). Light and dark blue squares represent Cu(II)O_2 plaquettes on different sublattices; green dots represent Li ions. The nonmagnetic UC is drawn in gray. Unfolded DFT + U band structure of (c) Cu_4O_3 without Li, magnetism and Hubbard-U; of (d) $LiCu_3O_3$, without magnetism and Hubbard-U; of (e) Cu_4O_3 with magnetism and Hubbard-U; and of (f) $LiCu_3O_3$ with AFM ordering plus Hubbard-U correlations. The color code in panels (c)–(f) was adapted to the one in Figs. 2 and 3, with yellow corresponding to no and blue corresponding to a strong spectral weight.

energetically most compelling [18]. Taking this structure as a pragmatic basis to rationalize the interplay of magnetic order and Li substitution in $LiCu_3O_3$, we calculate the electronic structure of fictitious Cu_4O_3 with all Li sites replaced by Cu(II) while maintaining the structure, and then introduce Li and electron correlation step by step. Figure 4(c) shows a DFT calculation of nonmagnetic Cu_4O_3, yielding the metallic band structure expected for uncorrelated electrons. Introducing the Li according to the ordering geometry in Fig. 4(b) while still refraining from correlations produces an upward shift of bands in (d), but leaves the overall band order unaltered [18]. In contrast, the experimentally determined magnetic order [18] plus Hubbard corrections open a gap in Fig. 4(e), yet, leave this magnetic Cu_4O_3 system still metallic within a realistic 2 eV $\leq U_{\mathrm{eff}} \leq$ 8 eV range of the effective on-site Coulomb potential. At last, only the cooperation of *both* Li *and* correlation plus magnetism pushes E_F into the band gap and produces a physical picture in Fig. 4(f) that is consistent with our ARPES experiment.

The authors thank Helmuth Berger, Philippe Bugnon, Daniel Petitgrand, Yusuke Nomura, and Silke Biermann for assistance in the initial stages of the project, as well as Sergio Ciuchi and Louk Rademaker for valuable discussions and feedback on this manuscript. Funding support came from the Swiss National Science Foundation under Grant No. P300P2-171221 (S. M.) and through its Sinergia network Mott Physics Beyond the Heisenberg Model. Further funding support came from the Deutsche Forschungsgemeinschaft (DFG, German Research Foundation) under Germany's Excellence Strategy through the Würzburg-Dresden Cluster of Excellence on Complexity and Topology in Quantum Matter ct.qmat (EXC 2147, Project ID 390858490) and through the Collaborative Research Centers SFB 1170 ToCoTronics (Project ID 258499086). The authors also acknowledge the Gauss Centre for Supercomputing e.V. for providing computing time on the GCS Supercomputer SuperMUC at Leibniz Supercomputing Centre. This research further used resources of the Advanced Light Source, which is a DOE Office of Science User Facility under Contract No. DE-AC02-05CH11231. The research leading to these results has also received funding from the European Union's Horizon 2020 research and innovation program under the Marie Skłodowska-Curie Grant Agreement No. 897276. Additionally, this work is based on experiments performed at the Swiss spallation neutron source SINQ, Paul Scherrer Institute, Villigen, Switzerland.

*simon.moser@uni-wuerzburg.de

[1] J. Ghijsen, L. H. Tjeng, J. van Elp, H. Eskes, J. Westerink, G. A. Sawatzky, and M. T. Czyzyk, Phys. Rev. B **38**, 11322 (1988).
[2] J. Zaanen, G. Sawatzky, and J. Allen, J. Magn. Magn. Mater. **54-57**, 607 (1986).
[3] F. C. Zhang and T. M. Rice, Phys. Rev. B **37**, 3759 (1988).
[4] H. Eskes and G. A. Sawatzky, Phys. Rev. Lett. **61**, 1415 (1988).
[5] H. Ebrahimnejad, G. A. Sawatzky, and M. Berciu, Nat. Phys. **10**, 951 (2014).
[6] P. W. Anderson, Phys. Rev. **79**, 350 (1950); **100**, 564 (1955); J. B. Goodenough, J. Phys. Chem. Solids **6**, 287 (1958); J. Kanamori, J. Phys. Chem. Solids **10**, 87 (1959).
[7] H. Eskes and G. A. Sawatzky, Phys. Rev. B **44**, 9656 (1991).

[8] B. O. Wells, Z. X. Shen, A. Matsuura, D. M. King, M. A. Kastner, M. Greven, and R. J. Birgeneau, Phys. Rev. Lett. **74**, 964 (1995).

[9] Y. Mizuno, T. Tohyama, S. Maekawa, T. Osafune, N. Motoyama, H. Eisaki, and S. Uchida, Phys. Rev. B **57**, 5326 (1998).

[10] V. V. Mazurenko, S. L. Skornyakov, A. V. Kozhevnikov, F. Mila, and V. I. Anisimov, Phys. Rev. B **75**, 224408 (2007).

[11] A. A. Gippius, E. N. Morozova, A. S. Moskvin, A. V. Zalessky, A. A. Bush, M. Baenitz, H. Rosner, and S.-L. Drechsler, Phys. Rev. B **70**, 020406(R) (2004); S.-L. Drechsler, J. Richter, R. Kuzian, J. Málek, N. Tristan, B. Büchner, A. Moskvin, A. Gippius, A. Vasiliev, O. Volkova, A. Prokofiev, H. Rakoto, J.-M. Broto, W. Schnelle, M. Schmitt, A. Ormeci, C. Loison, and H. Rosner, J. Magn. Magn. Mater. **316**, 306 (2007), proceedings of the Joint European Magnetic Symposia.

[12] S. Moser, L. Moreschini, H.-Y. Yang, D. Innocenti, F. Fuchs, N. H. Hansen, Y. J. Chang, K. S. Kim, A. L. Walter, A. Bostwick, E. Rotenberg, F. Mila, and M. Grioni, Phys. Rev. Lett. **113**, 187001 (2014).

[13] C. P. J. Adolphs, S. Moser, G. A. Sawatzky, and M. Berciu, Phys. Rev. Lett. **116**, 087002 (2016).

[14] S. Moser, Y. Nomura, L. Moreschini, G. Gatti, H. Berger, P. Bugnon, A. Magrez, C. Jozwiak, A. Bostwick, E. Rotenberg, S. Biermann, and M. Grioni, Phys. Rev. Lett. **118**, 176404 (2017).

[15] S. Hibble, J. Köhler, A. Simon, and S. Paider, J. Solid State Chem. **88**, 534 (1990).

[16] R. Berger, P. Önnerud, and R. Tellgren, J. Alloys Compd. **184**, 315 (1992).

[17] A. A. Bush, K. E. Kamentsev, and E. A. Tishchenko, Inorg. Mater. **55**, 374 (2019).

[18] See Supplemental Material at http://link.aps.org/supplemental/10.1103/PhysRevLett.132.126502 for details, which includes Refs. [14–17,19–52].

[19] A. L. Efros and B. I. Shklovskii, J. Phys. C **8**, L49 (1975).

[20] B. I. Shklovskii and A. L. Efros, *Electronic Properties of Doped Semiconductors* (Springer-Verlag Berlin, Heidelberg, 1984), 10.1007/978-3-662-02403-4.

[21] M. Pollak, M. Ortuño, and A. Frydman, *The Electron Glass* (Cambridge University Press, Cambridge, England, 2012).

[22] R. Rosenbaum, Phys. Rev. B **44**, 3599 (1991).

[23] D. Joung and S. I. Khondaker, Phys. Rev. B **86**, 235423 (2012).

[24] V. Y. Butko, J. F. DiTusa, and P. W. Adams, Phys. Rev. Lett. **84**, 1543 (2000).

[25] M. Pollak, Discuss. Faraday Soc. **50**, 13 (1970).

[26] P. Fischer, G. Frey, M. Koch, M. Könnecke, V. Pomjakushin, J. Schefer, R. Thut, N. Schlumpf, R. Bürge, U. Greuter, S. Bondt, and E. Berruyer, Physica (Amsterdam) **276-278B**, 146 (2000).

[27] J. Rodríguez-Carvajal, Physica (Amsterdam) **192B**, 55 (1993).

[28] J. D. Axe and J. B. Hastings, Acta Crystallogr. Sect. A **39**, 593 (1983).

[29] J. G. Massey and M. Lee, Phys. Rev. B **62**, R13270 (2000).

[30] S. Khondaker, I. Shlimak, J. Nicholls, M. Pepper, and D. Ritchie, Solid State Commun. **109**, 751 (1999).

[31] A. M. Somoza, M. Ortuño, and M. Pollak, Phys. Status Solidi (c) **1**, 42 (2004).

[32] M. Ortuño, J. Talamantes, E. Cuevas, and A. Díaz-Sánchez, Philos. Mag. B **81**, 1049 (2001).

[33] A. Pérez-Garrido, M. Ortuño, E. Cuevas, J. Ruiz, and M. Pollak, Phys. Rev. B **55**, R8630 (1997).

[34] U. Kabasawa, Y. Tarutani, M. Okamoto, T. Fukazawa, A. Tsukamoto, M. Hiratani, and K. Takagi, Phys. Rev. Lett. **70**, 1700 (1993).

[35] D. A. Zakheim, I. V. Rozhansky, I. P. Smirnova, and S. A. Gurevich, J. Exp. Theor. Phys. **91**, 553 (2000).

[36] P. Sheng, B. Abeles, and Y. Arie, Phys. Rev. Lett. **31**, 44 (1973).

[37] P. Sheng, Phys. Rev. B **21**, 2180 (1980).

[38] H. M. Rønnow, C. Renner, G. Aeppli, T. Kimura, and Y. Tokura, Nature (London) **440**, 1025 (2006).

[39] K. Behnia, *Fundamentals of Thermoelectricity* (Oxford University Press, New York, 2015).

[40] R. P. Wang, H. Jin, H. Sekine, H. Maeda, and Y. Tanaka, J. Phys. Condens. Matter **9**, 9615 (1997).

[41] T. L. Aselage, D. Emin, S. S. McCready, and R. V. Duncan, Phys. Rev. Lett. **81**, 2316 (1998).

[42] R. B. Lehoucq, D. C. Sorensen, and C. Yang, *ARPACK Users' Guide, Software, Environments, and Tools* (Society for Industrial and Applied Mathematics, Philadelphia, 1998).

[43] G. Kresse and J. Furthmüller, Phys. Rev. B **54**, 11169 (1996).

[44] K. Momma and F. Izumi, J. Appl. Crystallogr. **41**, 653 (2008).

[45] F. Izumi and K. Momma, *Solid State Phenom.* 130, 15 (2007).

[46] V. Wang, N. Xu, J.-C. Liu, G. Tang, and W.-T. Geng, Comput. Phys. Commun. **267**, 108033 (2021).

[47] J. P. Perdew, K. Burke, and M. Ernzerhof, Phys. Rev. Lett. **77**, 3865 (1996).

[48] A. Rohrbach, J. Hafner, and G. Kresse, J. Phys. Condens. Matter **15**, 979 (2003).

[49] O. Bengone, M. Alouani, P. Blöchl, and J. Hugel, Phys. Rev. B **62**, 16392 (2000).

[50] A. I. Liechtenstein, V. I. Anisimov, and J. Zaanen, Phys. Rev. B **52**, R5467 (1995).

[51] E. Şaşıoğlu, C. Friedrich, and S. Blügel, Phys. Rev. B **83**, 121101(R) (2011).

[52] M. Tomić, H. O. Jeschke, and R. Valentí, Phys. Rev. B **90**, 195121 (2014).

[53] A. L. Efros, J. Phys. C **9**, 2021 (1976).

[54] J. S. Lim, J. H. Lee, A. Ikeda-Ohno, T. Ohkochi, K.-S. Kim, J. Seidel, and C.-H. Yang, Phys. Rev. B **94**, 035123 (2016).

[55] T. Chen and B. Skinner, Phys. Rev. B **94**, 085146 (2016).

[56] N. Papadopoulos, G. A. Steele, and H. S. J. van der Zant, Phys. Rev. B **96**, 235436 (2017).

[57] B. Rachmilowitz, H. Zhao, Z. Ren, H. Li, K. H. Thomas, J. Marangola, S. Gao, J. Schneeloch, R. Zhong, G. Gu, C. Flindt, and I. Zeljkovic, npj Quantum Mater. **5**, 72 (2020).

[58] P. D. C. King, T. D. Veal, and C. F. McConville, Phys. Rev. B **77**, 125305 (2008).
[59] S. Doniach and M. Sunjic, J. Phys. C **3**, 285 (1970).
[60] S. Moser, J. Electron Spectrosc. Relat. Phenom. **214**, 29 (2017).
[61] Apart from an umklapp band that is observed only in $LiCu_2O_2$ [14].
[62] S. Souma, L. Chen, R. Oszwałdowski, T. Sato, F. Matsukura, T. Dietl, H. Ohno, and T. Takahashi, Sci. Rep. **6**, 27266 (2016).
[63] Y.-H. Song, Z.-Y. Jia, D. Zhang, X.-Y. Zhu, Z.-Q. Shi, H. Wang, L. Zhu, Q.-Q. Yuan, H. Zhang, D.-Y. Xing, and S.-C. Li, Nat. Commun. **9**, 4071 (2018).